applied sciences

MDPI

Article

Assessing Cardiac Sympatho-Vagal Balance Through Wavelet Transform Analysis of Heart Rate Variability

A.M. Nelushi [1], C.H. Manathunga [1,2,3,*], N.G.S. Shantha Gamage [1] and Tadachika Nakayama [2,3,*]

[1] Department of Physics, Faculty of Applied Sciences, University of Sri Jayewardenepura, Nugegoda 10250, Sri Lanka; nelushiadhikari@gmail.com (A.M.N.); shanthagamage@sci.sjp.ac.lk (N.G.S.S.G.)
[2] Department of Science and Technology Innovation, Nagaoka University of Technology, 1603-1, Kamitomioka, Nagaoka 940-2188, Niigata, Japan
[3] Extreme Energy–Density Research Institute (EDI), Nagaoka University of Technology, 1603-1, Kamitomioka, Nagaoka 940-2188, Niigata, Japan
* Correspondence: s245001@stn.nagaokaut.ac.jp or chandimavc@sjp.ac.lk (C.H.M.); nky15@vos.nagaokaut.ac.jp (T.N.)

Abstract: Heart rate variability (HRV), which is the variation between consecutive heartbeats, reflects the electrical activity of the heart and provides insight into the autonomic nervous system (ANS) function. This study uses wavelet transform-based HRV feature extraction to investigate cardiac sympatho-vagal balance. Both the continuous wavelet transform (CWT) and discrete wavelet transform (DWT) methods were applied in different steps. DWT was used for R-peak detection and CWT and MODWT were used to generate spectrograms from RR intervals. Frequency components (HF, LF, and VLF) within 0.003–0.4 Hz were extracted, and power estimation was performed. The LF/HF ratio, indicating sympatho-vagal balance, was calculated. ECG data from 42 arrhythmia patients and 18 normal sinus rhythm subjects were analyzed. The results showed a lower LF/HF ratio in arrhythmia patients, with higher HF power in arrhythmia subjects and higher LF power in normal sinus rhythm subjects. The study suggests that the parasympathetic nervous system dominates the ANS in arrhythmia patients, while the sympathetic nervous system dominates in normal sinus rhythm patients.

Keywords: arrhythmia; heart rate variability; LF/HF ratio; sympatho-vagal balance; wavelet transform

Academic Editor: Vladislav Toronov

Received: 10 January 2025
Revised: 1 February 2025
Accepted: 4 February 2025
Published: 7 February 2025

Citation: Nelushi, A.M.; Manathunga, C.H.; Shantha Gamage, N.G.S.; Nakayama, T. Assessing Cardiac Sympatho-Vagal Balance Through Wavelet Transform Analysis of Heart Rate Variability. *Appl. Sci.* **2025**, *15*, 1687. https://doi.org/10.3390/app15041687

1. Introduction

The human heart is crucial for sustaining life by pumping blood and delivering oxygen. Its rhythmic contractions, regulated by the autonomic nervous system (ANS), are influenced by the balance between the sympathetic nervous system (SNS) and the parasympathetic nervous system (PNS). This balance is called sympatho-vagal balance, and significantly impacts heart rate variability (HRV), a key biomarker for cardiovascular [1]. HRV reflects fluctuations in the intervals between heartbeats and indicates the dynamic interaction between SNS and PNS. Healthy HRV shows good autonomic adaptability, while reduced HRV is linked to conditions like stress, cardiovascular diseases, and metabolic disorders [2].

The clinical significance of HRV was first introduced by Hon and Lee in 1965 by observing that variation in interbeat intervals preceded instances of fetal distress and variations in overall heart rate [3]. Since then, numerous research studies have been conducted to discover the connections between various diseases and heart rate variability. Research has shown that reduced HRV is correlated with an increased risk of cardiovascular disease, which remains a leading cause of mortality worldwide [4–6]. A correlation of HRV

to mental health conditions such as depression and anxiety was found as lower HRV is associated with higher risks of myocardial infarction and coronary heart disease [7–9]. HRV is influenced by other factors than diseases including age [10,11], gender [12–14], lifestyle factors such as smoking [15] and alcohol [16], and environmental factors such as social stress, noise, and air pollutants [17].

Electrocardiography (ECG) records the electrical activity of the cardiac system as a signal [3] and provides data for HRV analysis. HRV exhibits abrupt changes in frequency throughout the ECG signal. According to the previous studies, HRV analysis using FT (Fourier transform) and STFT (short-term Fourier transform) has not resulted in positive outcomes due to their limitations such as not being localized in the time domain and having a fixed window size [18,19]. Wavelet transform analysis has emerged as a powerful tool for analyzing HRV and assessing cardiac sympatho-vagal balance with both time- and frequency-localized multi-resolution analysis [20].

1.1. Wavelet Transformation

The wavelet theory was first proposed by the geophysicist Jean Morlet and the theoretical physicist Alex Grossmann in 1981. These wavelets are generated from a single function called "Mother Wavelet" which produces a family of functions by translation and dilation. The mother wavelet $\psi(t)$ is given by the following equation [21]:

$$\psi_{a,b}(t) = \frac{1}{\sqrt{|a|}}\psi\left(\frac{t-b}{a}\right);\ a,b \in \mathbb{R}, a \neq 0 \tag{1}$$

where a is the scaling parameter and b is the translational parameter. The time widths of wavelets are adapted to their frequencies.

1.1.1. Wavelets

There are various wavelet families, including Morlet, Haar, Daubechies, Symlets, Gaussian, Mexican Hat, Mayer, and Biorthogonal wavelets. The wavelet chosen depends on the signal being processed. For ECG signal processing, Daubechies and Symlet wavelets are often used due to their similarity to the ECG waveform QRS complex [22–26]. The Daubechies family has 20 types (e.g., db2, db3, and db4), and the Symlet family has 19 types (e.g., sym3, sym4, and sym6). Figure 1 shows the db4 and sym4 wavelets used for ECG analysis.

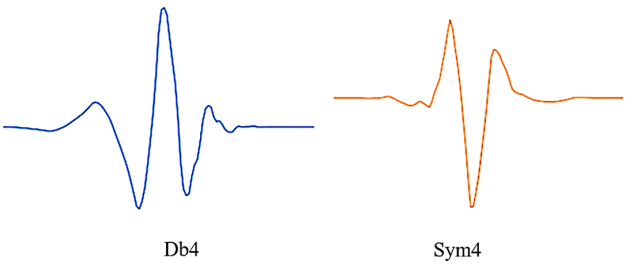

Figure 1. db4 and sym4 wavelets. The sym4 wavelet is from the Symlet family, and db4 is from the Daubechies family. These wavelets show similarities with the ECG signal waveform and are used in analyzing the ECG signal waveforms.

1.1.2. Continuous Wavelet Transform (CWT)

Continuous wavelet transform is the convolution of the signal x(t) with the scaled and translated version of the mother wavelet function Ψ(t). CWT is given by the following equation:

$$X(a,b,t) = \int_{-\infty}^{+\infty} x(t) \cdot \frac{1}{\sqrt{|a|}}\Psi\left(\frac{t-b}{a}\right)dt \tag{2}$$

where a is the scaling parameter and b is the translational parameter.

CWT is used in time-frequency analysis to process spectrograms and filtering purposes of time-localized frequency components.

1.1.3. Discrete Wavelet Transform (DWT)

Discrete wavelet transform (DWT) is the discretized scaled and translated version of the mother wavelet Ψ(t). DWT is given by the following equation:

$$X(a,b,t) = \sum_{m=0}^{p-1} x(t_m) \cdot \frac{1}{\sqrt{|a|}} \Psi\left(\frac{t_m - b}{a}\right) \quad (3)$$

In CWT, the integral is replaced with a summation as discrete values are considered. In DWT, the discrete values are represented as $a = k2^j$ and $b = 2^j$, where the dyadic power improves the efficiency of the analysis. DWT is used in multi-resolution analysis for tasks like signal denoising and signal compression [27,28].

1.1.4. Multi-Resolution Analysis

Wavelet analysis is a multi-resolution technique in both the time and frequency domains, offering good localization in both. It provides better time resolution for higher frequencies and better frequency resolution for lower frequencies, as shown in Figure 2a. High frequencies require good time resolution, achieved using narrow wavelets, while low frequencies spread over longer time durations, requiring wider wavelets for better frequency resolution [29].

1.1.5. Multilevel Decomposition

Multilevel decomposition is a technique for filtering the high- and low-frequency components of a signal at multiple levels. At each level, the signal is split into detail coefficients (high-frequency) and approximation coefficients (low-frequency). The approximation coefficients capture the low-frequency components, while the detail coefficients capture the high-frequency components [30].

This is achieved by applying low-pass and high-pass filters (LPF and HPF) at each level. LPF captures lower frequencies while rejecting higher ones, and HPF captures higher frequencies while rejecting lower ones [31]. In Figure 2b, approximation and detail coefficients are represented by "A" and "D", respectively. The approximation coefficients are iteratively filtered at each level in a dyadic process.

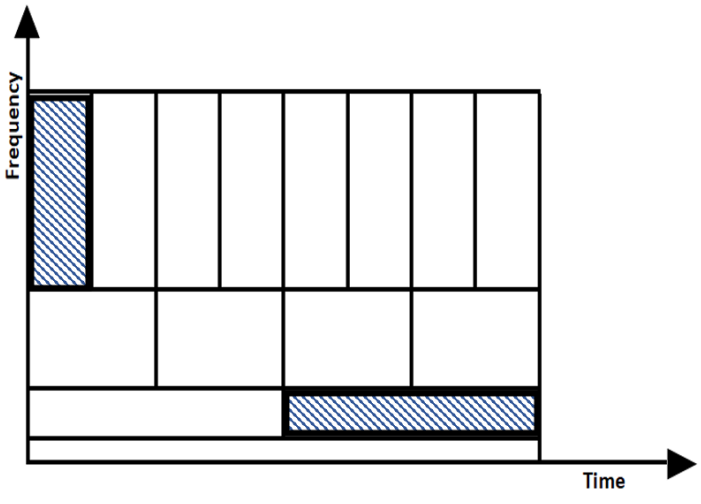

(**a**)

Figure 2. *Cont.*

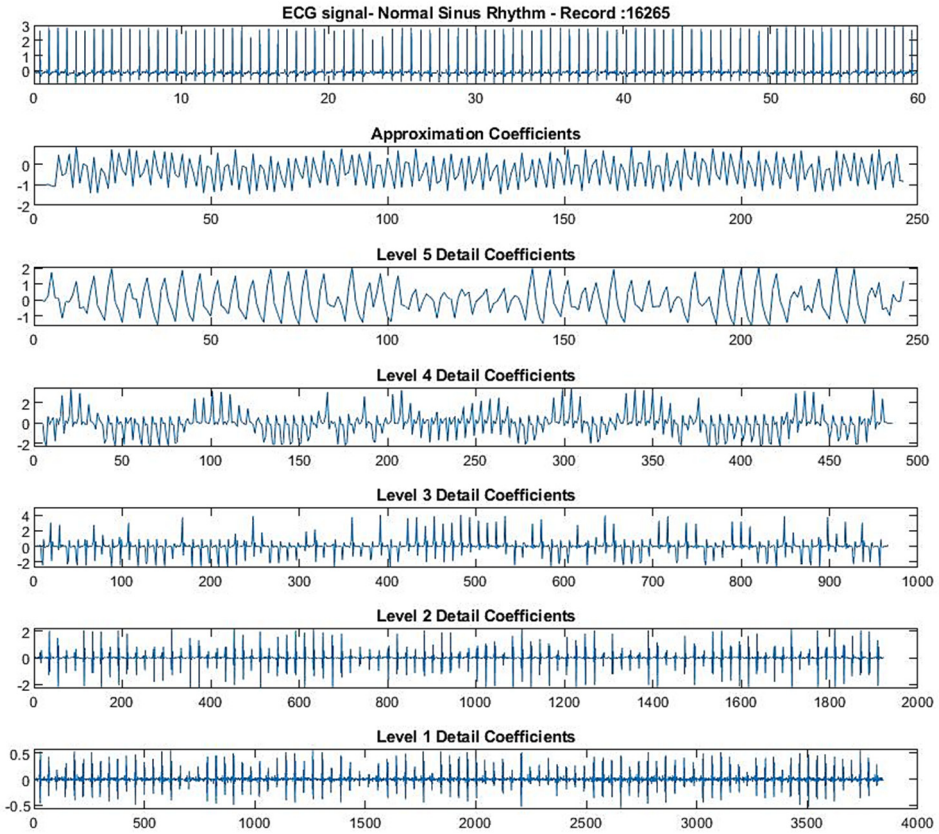

(**b**)

Figure 2. (**a**) Graphical representation of multi-resolution analysis. Wider wavelets (windows) are used in multi-resolution analysis to capture lower frequencies which provide high frequency resolution, and narrow wavelets (windows) are used to capture higher frequencies which provide high time resolution. (**b**) Multilevel decomposition. The approximation coefficients are shown by "A" and detailed coefficients are shown by "D". At each level the number of coefficients is halved.

2. Materials and Methods

ECG data for an HRV analysis were sourced from the trusted PhysioNet database [32], specifically the MIT-BIH Normal Sinus Rhythm and MIT-BIH Arrhythmia Databases. The Normal Sinus Rhythm Database includes 18 ECG recordings from patients referred to Beth Israel Deaconess Medical Center who have not exhibited significant arrhythmias, and involves 5 men aged from 26 to 45 and 13 women aged from 20 to 50. The recordings were sampled at a sampling rate of 128 Hz. The Arrhythmia Database consists of 24 h ambulatory ECG recordings of 47 patients, sampled at 360 Hz with 11-bit resolution [33].

The databases provide recordings in multiple formats (.atr, .dat, .hea, and .xws), which were challenging to handle. To ease processing, PhysioBank ATM offered ECG data in the more MATLAB-compatible .mat format. The process involved selecting the database and recording, setting the length to 1 h, and exporting both .mat and .info files.

The .info file contains crucial data such as gain, base value, sampling frequency, and sampling time, which are needed for ECG waveform plotting.

The analysis was performed using MATLAB 2021a, selecting 18 recordings from the Normal Sinus Rhythm and 46 from the Arrhythmia database. The MLII channel (lead II) ECG signal was chosen for the Arrhythmia dataset and the ECG1 signal for the Normal Sinus Rhythm dataset. Data from the .info files (sample rate, gain, and base values) were used in the analysis, with each step of the signal processing performed using self-written code (Figure 3).

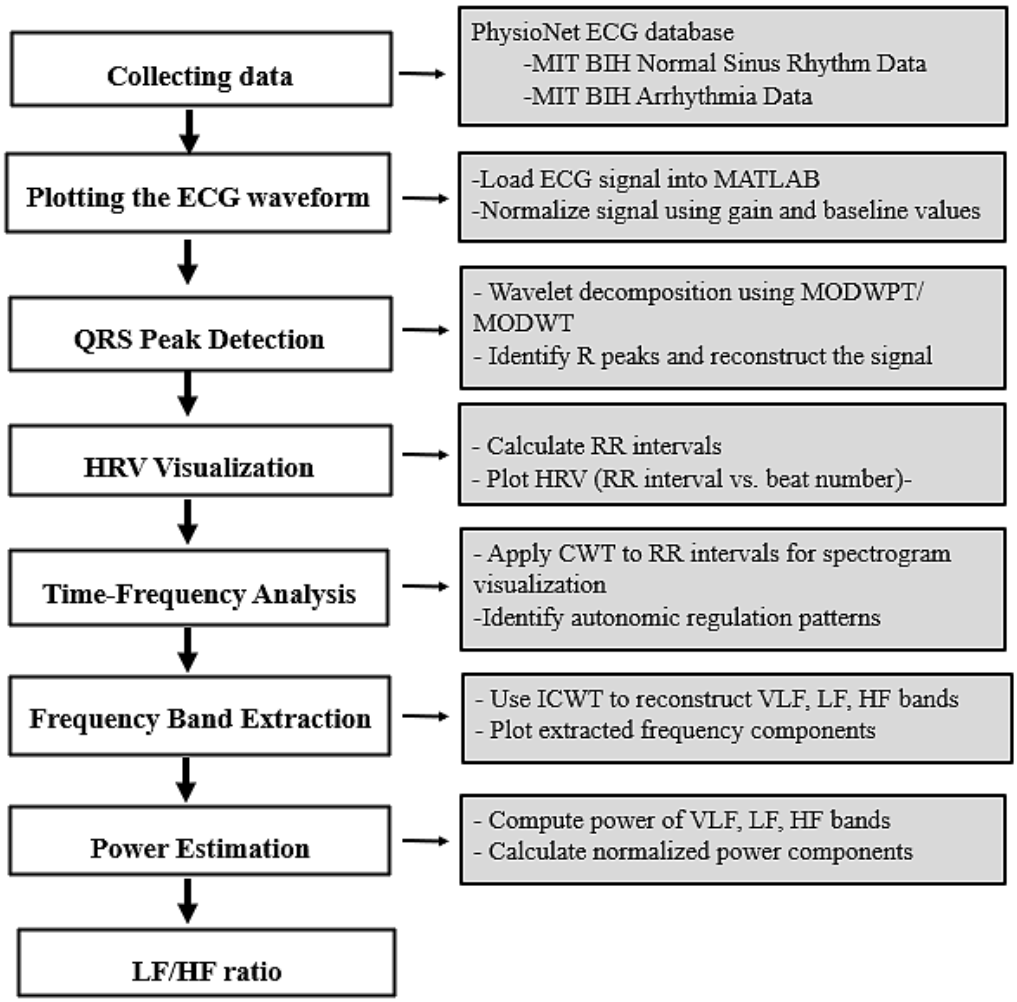

Figure 3. Methodology flowchart. This illustrates the multi-step process of HRV analysis.

The ECG signal data were loaded into MATLAB using the command ecg=load('16,265m.mat'), and the sampling rate, total number of samples, gain, and baseline were defined according to the .info file. Each ECG signal was normalized for consistency using the formula ecgsignal = ((ecg.val) − base)/gain. A time vector was created corresponding to each sample point, and the ECG signal was plotted against this vector, comparing it with the waveform from PhysioBank ATM.

The next step involved locating the QRS complexes. Bandpass filtering was applied to identify R peaks within the QRS complexes, which contain middle frequencies in the ECG signal. There are many research studies conducted on detecting QRS complexes using wavelet transform. In those studies, the most common method of detecting QRS complex is using maximum overlap discrete wavelet transform (MODWT) or maximum overlap discrete wavelet packet transform (MODWPT) [22–24]. For this study, the maximal overlap discrete wavelet transform (MODWT) was used for wavelet decomposition. Different sampling frequencies in the Normal Sinus Rhythm and Arrhythmia datasets required different levels of decomposition. Previous studies have identified the QRS complex within the 0–50 Hz frequency range [34].

The MIT BIH normal sinus dataset, with a sampling frequency of 128 Hz, was analyzed using the MODWT, computed down to 5 levels with the db4 wavelet. The corresponding

frequency bands are shown in Table 1. The detail coefficients from levels 2, 3, 4, and 5 were retained, while the others were set to zero using the following code:

```
wt = modwt(ecgsignal,5,'db4');

wtrec = zeros(size(wt));

wtrec(2:3:4:5,:) = wt(2:3:4:5,:);
```

Table 1. Frequency ranges for each level in DWT (sampling frequency 128 Hz).

Level	Scale	Frequency Band (Hz)
1	2	64–128
2	4	32–64
3	8	16–32
4	16	8–16
5	32	4–8

Next, R peaks were isolated, and the inverse MODWT was applied to reconstruct the signal:

```
y = imodwt(wtrec,'db4');
```

To obtain positive peaks, the squared magnitude of the reconstructed signal was taken. R peaks were located using the findpeaks() function, with minimum peak distance and height determined by plotting the reconstructed signal. These values were applied to findpeaks() to identify the QRS peak position, time location, and isolated R peaks, which were then plotted (Figure 4).

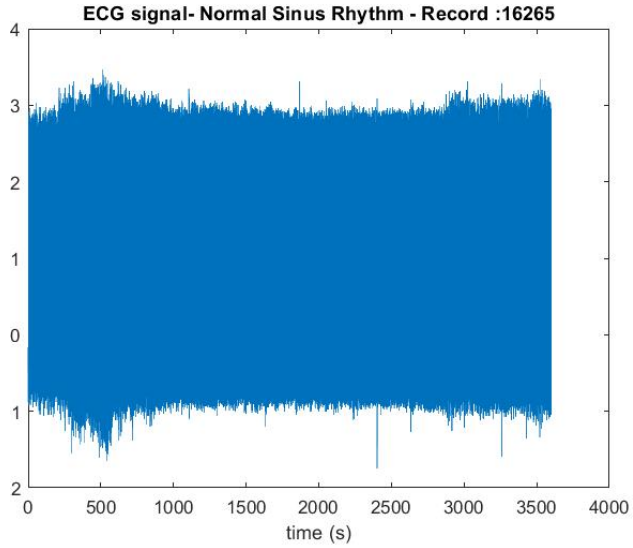

Figure 4. ECG signal of normal sinus rhythm recording—16,265. The Y-axis represents the voltage amplitudes of the ECG signal and the x-axis represents the time duration of the ECG signal.

For the MIT BIH Arrhythmia dataset, with a sampling frequency of 360 Hz, the MODWT was computed down to 6 levels using the sym4 wavelet, providing the frequency bands shown in Table 2. Detail coefficients from levels 3, 4, 5, and 6 were retained, and the others were set to zero. The reconstructed signal was generated using IMODWT with the sym4 wavelet. The same R peak localization procedure as in the normal sinus dataset analysis was followed.

Table 2. Frequency ranges for each level in DWT (sampling frequency 360 Hz).

Level	Scale	Frequency Band (Hz)
1	2	90–180
2	4	45–90
3	8	22.5–45
4	16	11.25–22.5
5	32	5.625–11.25
6	64	2.8125–5.625

Additionally, MODWPT, another wavelet decomposition method, was used to locate R peaks following the same steps as in the MODWT method. The final step was to calculate HRV using RR intervals.

HRV analysis, a key objective of this study, involves calculating the variation between consecutive heartbeats, or the distance between R peaks (Figure 5). This was performed by using the following code:

$$\text{rr\_intervals} = \text{diff(locs)} \times 1000;$$

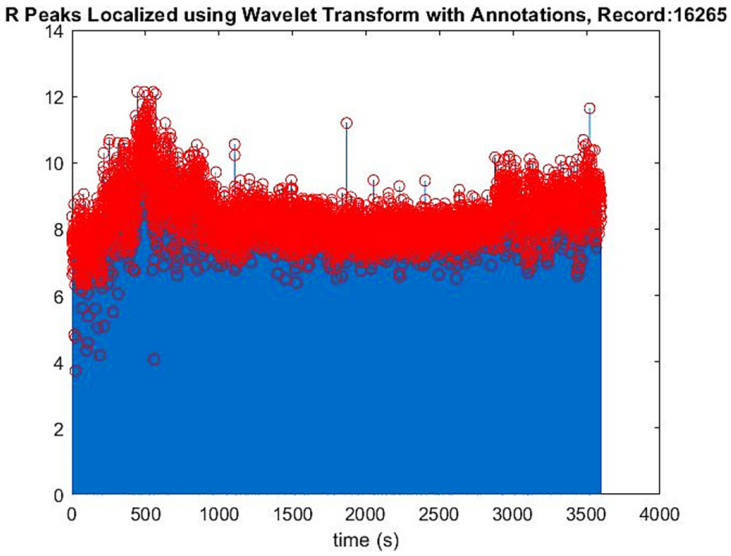

Figure 5. Reconstructed signal containing R peaks in red color annotations of record no. 16,265.

The difference between R peak time locations was used to compute the RR intervals. These values, initially in the millisecond range, were multiplied by 1000 to convert them into milliseconds. The RR interval values were then plotted against the beat number (Figure 6), representing HRV.

Next, the frequency components of the RR intervals were extracted using CWT for a time-frequency analysis. The sampling frequency and time vector of the RR intervals were calculated based on the number of RR intervals and the original ECG signal's sampling frequency:

$$\text{rr\_intervals\_Fs} = (\text{length(rr\_intervals)}/\text{length(samples)}) \times \text{Fs};$$

$$\text{rr\_intervals\_t} = (0{:}(\text{length(rr\_intervals)} - 1))/(\text{rr\_intervals\_Fs} \times 60);$$

The CWT spectrogram was then plotted using the cwt() function, as shown in Figure 7.

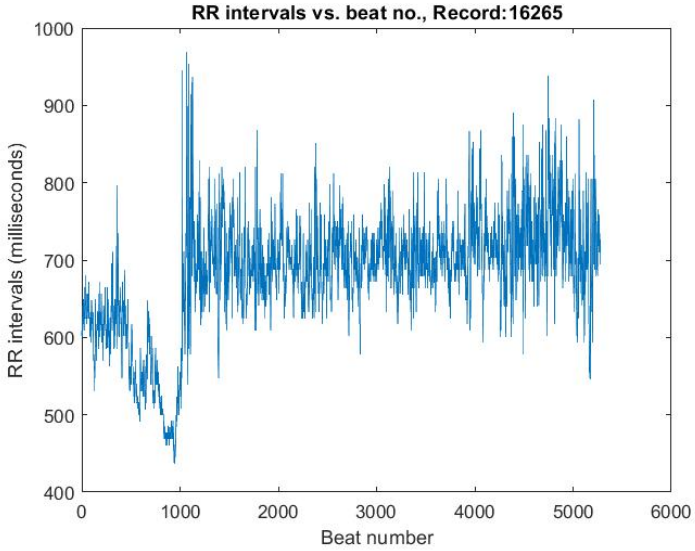

Figure 6. The graph of RR intervals vs. the beat number. This is the representation of variation in the heart rate, HRV.

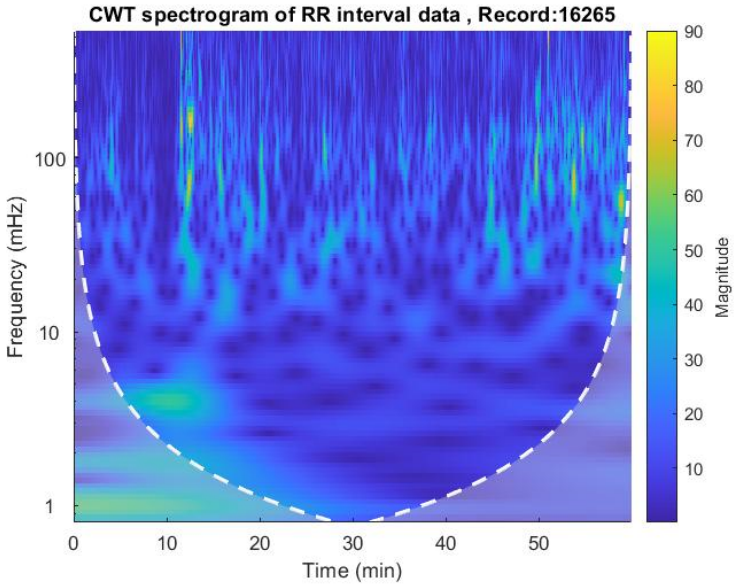

Figure 7. The CWT spectrogram of record no. 16,265. CWT spectrum represents 3 dimensions: frequency, time, and the RR interval magnitude by each coordinate. The dashed line is the cone of influence which indicates the more accurate results inside the cone. We can observe high-magnitude events in bright colors in the spectrograms.

In the HRV analysis, the time-localized frequency components can be extracted by applying inverse continuous wavelet transform (ICWT) to the ECG signal [35]. This was carried out by reconstructing the long-term ECG signal for each frequency band separately. ECG signal is divided into 4 major frequency bands: ultra-low frequency (LF), very low frequency (VLF), low frequency (LF), and high frequency (HF) (Figure 8). These frequency band values are different for short-term and long-term ECG signals. For short-term ECG signals, the frequency bands are defined as VLF $\leq$ 0.04 Hz, LF range: 0.04–0.15 Hz, and HF range: 0.15–0.4 Hz. For long-term ECG signals, the frequency bands are defined as ULF $\leq$ 0.003 Hz, VLF range: 0.003–0.04 Hz, LF range: 0.04–0.15 Hz, and HF range–0.15–0.4 Hz [36].

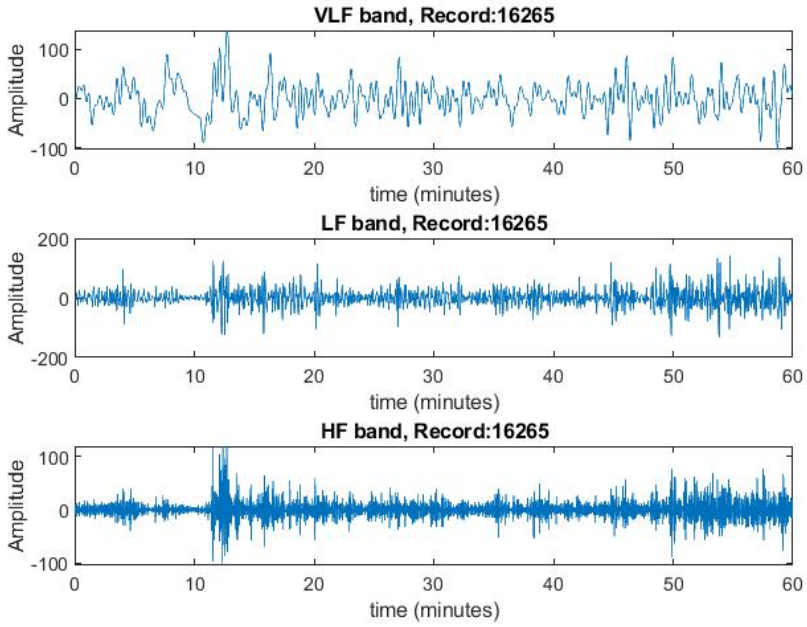

Figure 8. Extracted frequency components in VLF, LF, and HF bands for record no. 16,265 from the spectrogram. This represents the variation in the magnitude of rr intervals for each band.

These extracted frequency components were then plotted separately against time.

The next step was to calculate the power of the VLF, LF, and HF bands. This was performed by calculating the square of the root mean square (RMS) values of the reconstructed signals for each frequency band:

```
power_VLF = rms(vlf_reconstruct)^2;
```

The total power was then obtained by summing the powers of the VLF, LF, and HF bands. To facilitate comparison, the power values were normalized by dividing them by the total power. The LF/HF ratio was then computed by dividing the normalized power of the LF band by the normalized power of the HF band.

3. Results and Discussion

Electrocardiography (ECG) is a non-invasive method used to assess cardiac health by capturing the heart's electrical activity. Wavelet transformation is a promising technique for analyzing ECG signals, providing insights into heart rate variability (HRV).

This study analyzed HRV using wavelet transformation on 60 ECG recordings from the MIT-BIH Normal Sinus Rhythm and Arrhythmia databases. The analysis followed five main steps: locating R peaks, calculating RR intervals, generating spectrograms, extracting frequency bands, and determining the LF/HF ratio using both continuous wavelet transform (CWT) and discrete wavelet transform (DWT).

Accurately locating R peaks is crucial, as the RR interval accuracy depends on it. Previous studies showed that the MODWT and MODWPT methods were effective for R peak detection, with MODWPT offering better resolution. Thus, both methods were tested on six randomly selected recordings from both databases (Normal Sinus: 16,265, 16,786, and 19,140; Arrhythmia: 106, 112, and 117) to evaluate their performance.

Except for recording no. 117, no significant differences were observed in the R peak localization, RR intervals, and spectrogram plots generated using MODWPT and MODWT for these ECG recordings. This similarity is illustrated in recording no. 16,786 in Figures 9 and 10. The total power and LF/HF ratio of these recordings, computed using

both the MODWPT and MODWT methods, were nearly equal, except for recording no. 117, as shown in Table 3.

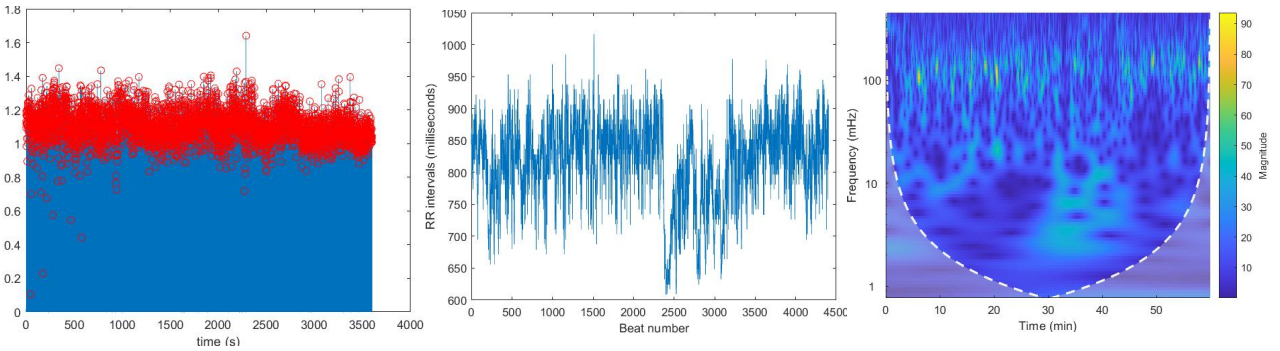

(**a**) (**b**) (**c**)

Figure 9. (**a**) Located R peaks. (**b**) RR interval vs. beat no. plot. (**c**) CWT spectrogram for record: 16,786 using MODWPT.

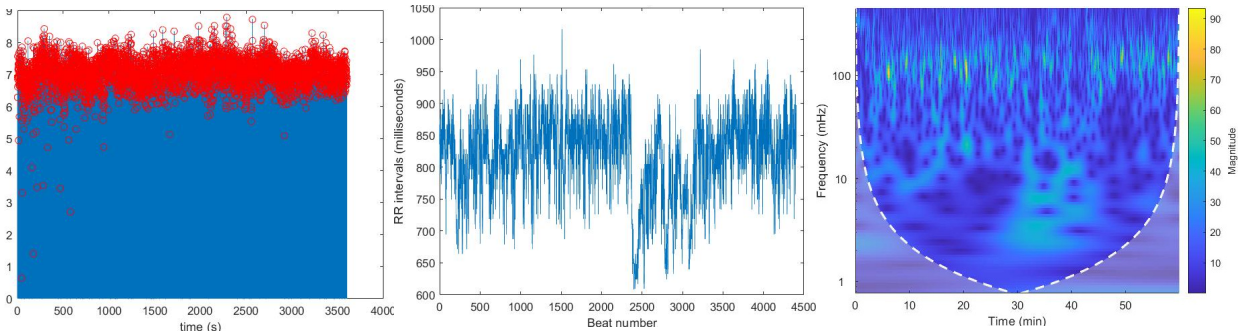

(**a**) (**b**) (**c**)

Figure 10. (**a**) Located R peaks. (**b**) RR interval vs. beat no. plot. (**c**) CWT spectrogram for record: 16,786 using MODWT. For recording no. 16,786, MODWPT method and MODWT method do not show any significant difference.

Table 3. Estimated LF/HF ratio values using MODWPT and MODWT methods.

	LF/HF Ratio					
Index / Method	16,265	16,786	19,140	106	112	117
MODWPT	3.188	1.869	1.682	0.103	1.032	0.424
MODWT	3.164	1.875	1.700	0.098	1.028	0.852

Figure 11a shows the R peak localization for recording no. 117 using MODWPT and MODWT, respectively, revealing a significant difference in R peak localization from beat 0 to 600. The RR interval vs. beat number plot for MODWPT (Figure 11b) also differs from the MODWT plot (Figure 12b) until the 600th beat. While the spectrograms from both methods show no significant difference (Figures 11c and 12c), the extracted frequency bands show a large difference in HF band power, confirming that MODWPT provides better resolution in the HF range than MODWT. This is because MODWPT decomposes both LF and HF components at each level, resulting in more filtered sub-frequency components, while MODWT only decomposes LF components. As a result, MODWPT offers better resolution in both LF and HF ranges, whereas MODWT performs better in LF components only.

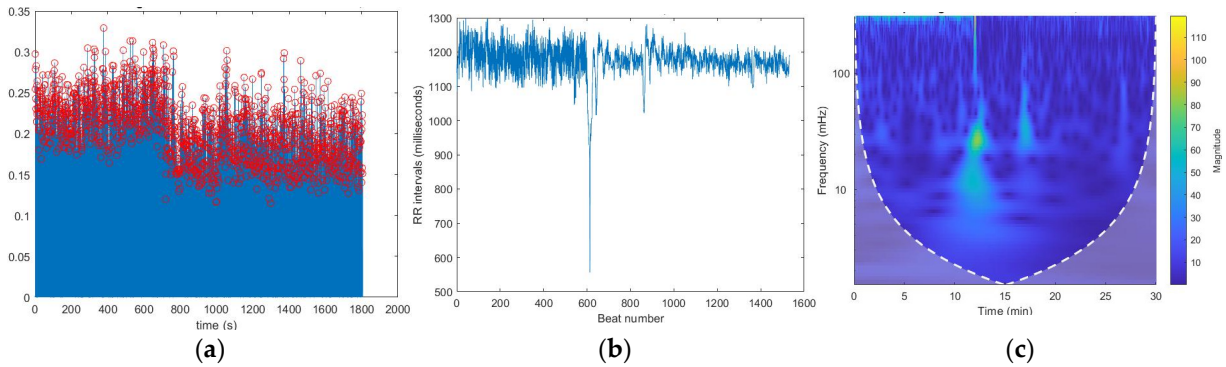

Figure 11. (**a**) Located R peaks. (**b**) RR interval vs. beat no. plot. (**c**) CWT spectrogram for the record: 117 using MODWPT. When comparing these plots with the MODWT method plots, we can observe a significant difference in the HF range until the 600 beat number.

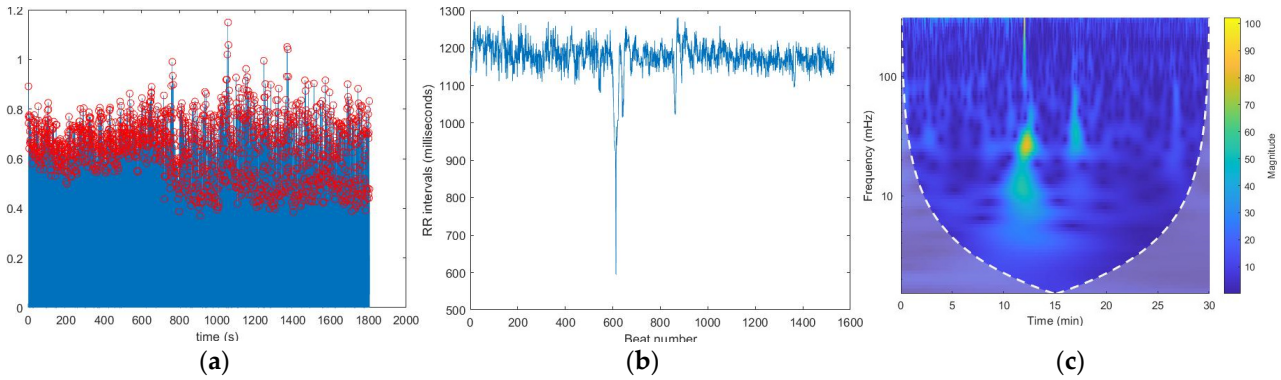

Figure 12. (**a**) Located R peaks. (**b**) RR interval vs. beat no. plot. (**c**) CWT spectrogram for record: 117 using MODWT.

However, the computational power required for MODWPT's multilevel decomposition leads to longer processing times, and in some cases, the analysis failed due to memory issues. Therefore, the study continued with the MODWT method.

For the analysis, the db4 and sym4 wavelets were used, as they resemble the QRS complex. The signals from the MIT-BIH normal sinus dataset were decomposed into five levels using db4, considering levels 2 to 5 for R peak localization. MIT-BIH arrhythmia signals were decomposed into six levels using sym4, with levels 3–6 considered. R peaks correspond to middle frequencies in the ECG signal, and previous studies suggest a sampling frequency of around 50 Hz for QRS peaks, explaining the exclusion of higher frequency levels.

During the R peak localization process, missing R peaks were observed in normal sinus ECG recordings (no: 16,420 and 16,483) and arrhythmia ECG recordings (no: 101, 111, 121, 201, and 234). These missing peaks are highlighted in Figure 13 with a yellow circle.

The missing peaks in the analysis were likely caused by selecting inappropriate values for the "MinPeakDistance" and "MinPeakHeight" parameters in the "findpeaks" MATLAB function or by data loss during the initial R peak localization process. These missing peaks lead to erroneous higher RR intervals. When a peak is missing, the gap between the neighboring R peaks increases, resulting in an incorrectly calculated maximum interval. Figure 14 shows the RR interval plots for recordings no. 16,420 and 121, highlighting the incorrect higher RR intervals due to these missing peaks.

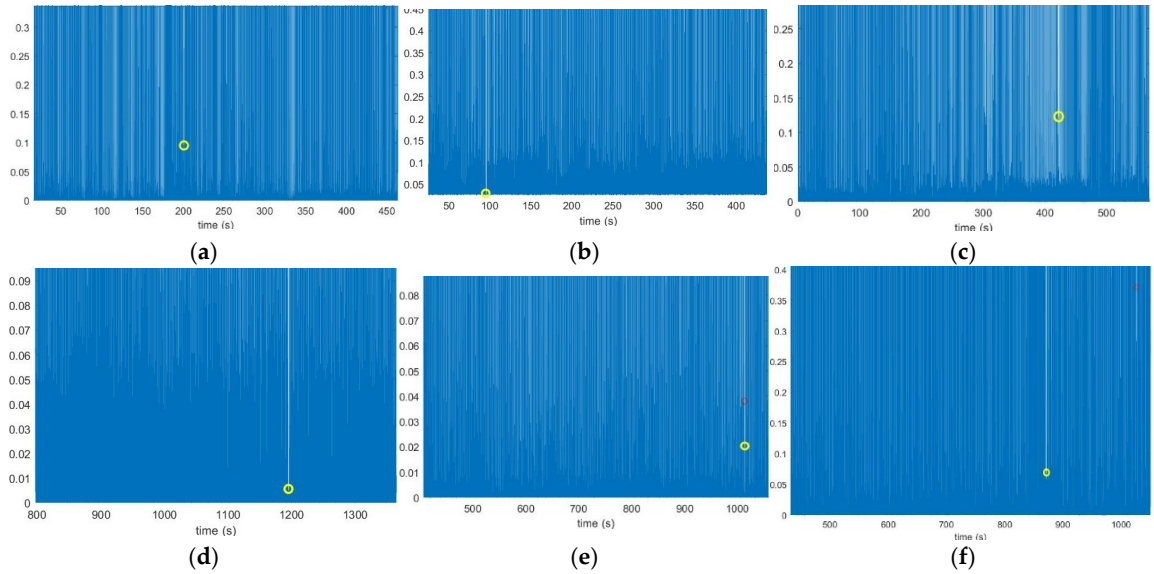

Figure 13. Missing peaks observed in the R peaks plot of recording: (**a**) 16,420, (**b**) 16,483, (**c**) 101, (**d**) 111, (**e**) 121, and (**f**) 234. These plots show the missed R peak circled in yellow color.

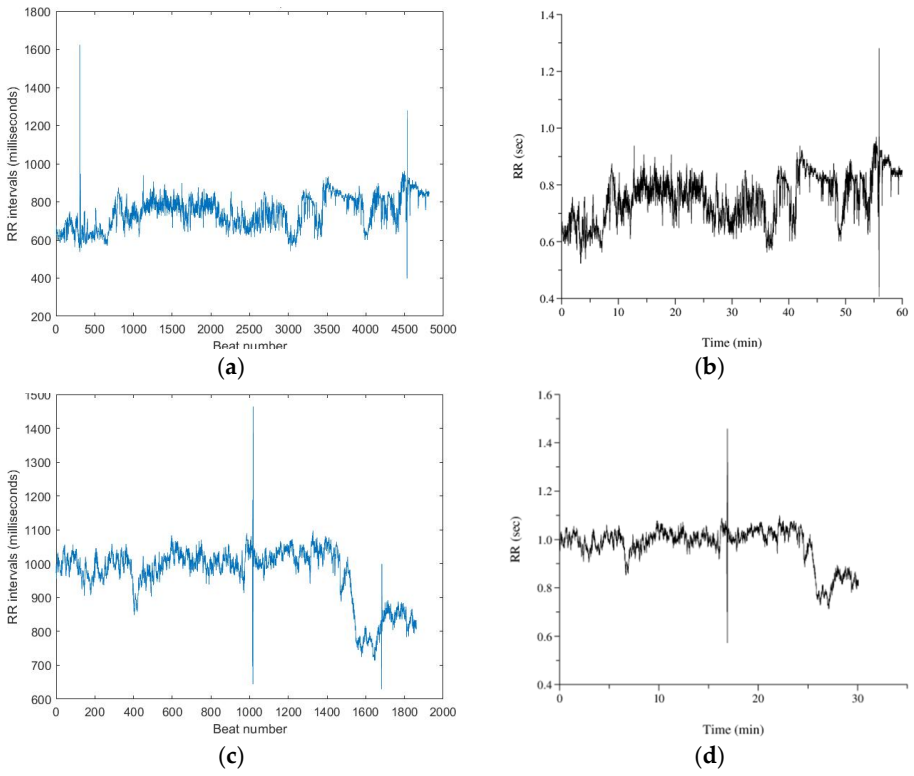

Figure 14. The RR interval plot of recording: (**a**) 16,420 observed with an incorrect higher interval between R peaks; (**b**) 16,420 obtained from the PhysioNet Database; (**c**) 121 observed with an incorrect higher interval between R peaks; (**d**) 121 obtained from the PhysioNet Database.

Adjusting the minimum distance and height of the R peaks did not resolve the issue and instead led to more incorrect higher RR intervals in the RR interval plots. It is important to note that reducing these parameters too much also caused incorrect R peak identification. For example, in Figure 13b, many peaks with higher amplitudes than the missing R peaks were identified, leading to incorrect R peak inclusion. After successfully locating R peaks, the RR intervals were calculated and plotted against the beat number. While some recordings showed incorrect higher intervals due to missing peaks, most recordings

produced accurate RR interval plots. Figure 15 shows the RR interval plots for recordings no. 16,786 and 115, which resemble the reference plots from PhysioBank ATM.

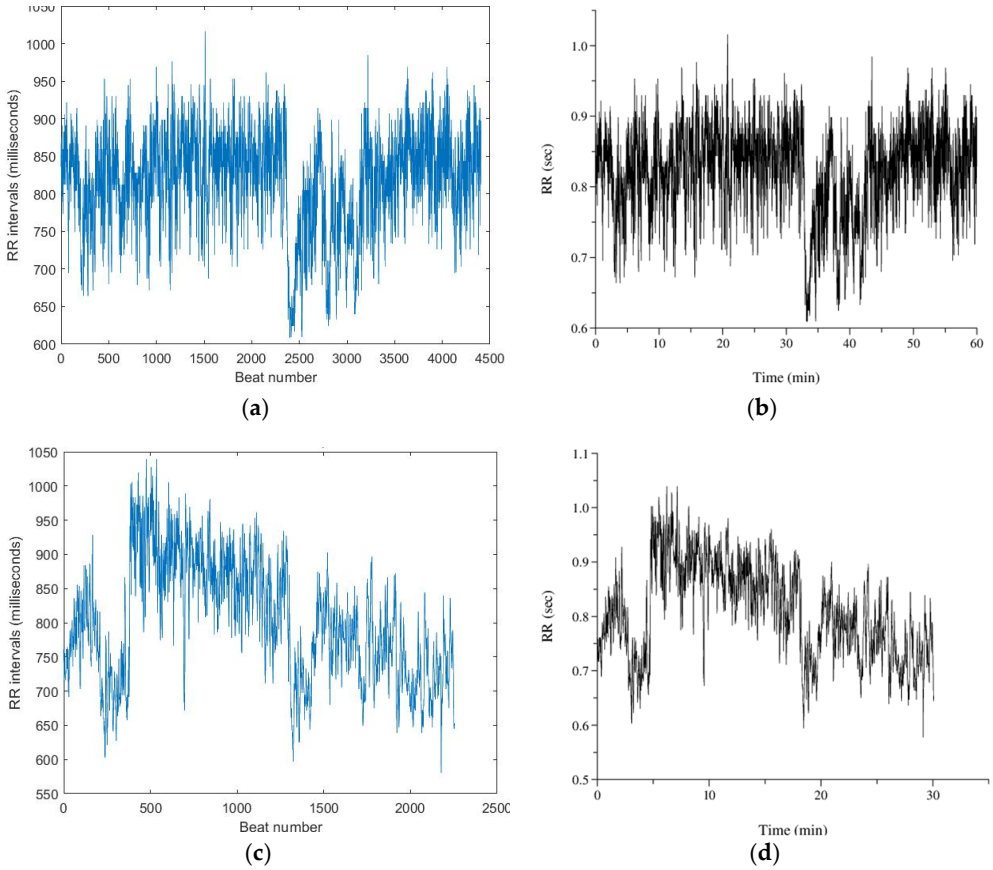

Figure 15. (**a**) RR interval plot of recording 16,786 plotted using MATLAB. (**b**) RR interval plot of recording 16,786 obtained from PhysioBank ATM. (**c**) RR interval plot of recording 230 plotted using MATLAB. (**d**) RR interval plot of recording 230 obtained from PhysioBank ATM.

For ECG recordings no. 16,773 (Figure 16b) and 18,784, the reference RR interval plots from PhysioBank ATM displayed interruptions in the middle section, raising doubts about their accuracy. Consequently, these plots were considered incorrect.

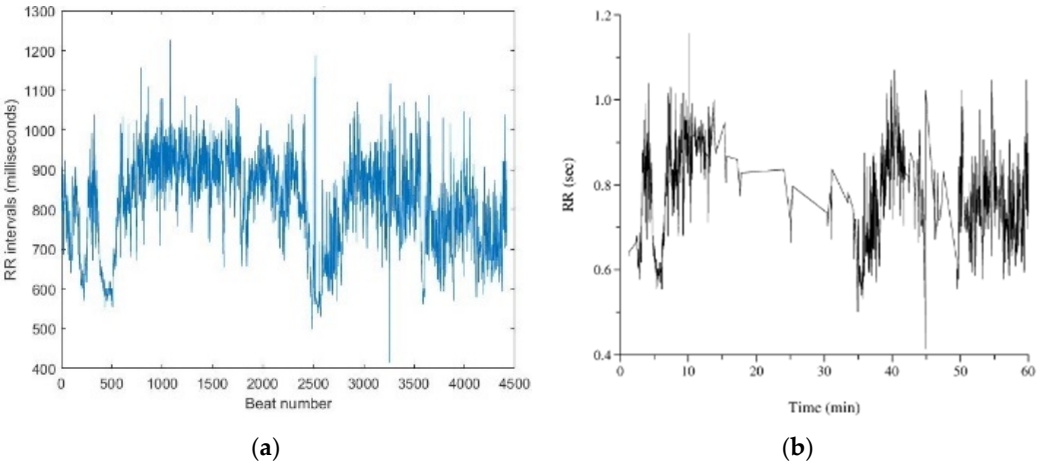

Figure 16. (**a**) RR interval plot of recording no. 16,773 plotted using MATLAB. (**b**) RR interval plot of recording no. 16,773 obtained from PhysioBank ATM.

Out of 60 recordings, only 7 showed inaccurate RR interval plots, so the study proceeded to the next steps of plotting spectrograms and extracting frequency components. CWT was applied to the RR interval signal to obtain spectrograms, where amplitude (energy) is represented by three dimensions: frequency increases along the y-axis, with lower-frequency components at the bottom. The cone of influence indicates more accurate data inside and less accurate data outside. The focus was on the HF, LF, and VLF components (0.003 Hz to 0.4 Hz). High-magnitude events were observed in some spectrograms, like for recordings 19,093 and 228, but the study's main interest was analyzing HRV data through these frequency bands reflecting ANS activity.

Figure 17a shows a spectrogram of a normal sinus rhythm ECG recording, where the LF and VLF ranges are brighter than the HF range, indicating higher LF power than HF power for this subject. This was consistent across all 18 normal sinus rhythm spectrograms. In contrast, Figure 17b illustrates an arrhythmia ECG recording, where the HF range is brighter, indicating higher HF power than LF power. This pattern was observed in almost all 42 arrhythmia spectrograms. However, some arrhythmia recordings (e.g., 112, 123, and 222) also showed bright areas in the LF range, as shown in Figure 18.

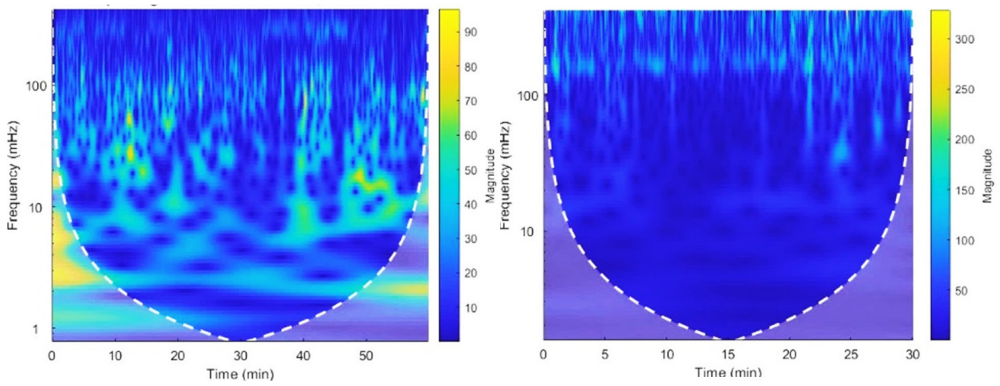

Figure 17. CWT spectrograms of recordings no. (**a**) 19,093 and (**b**) 228.

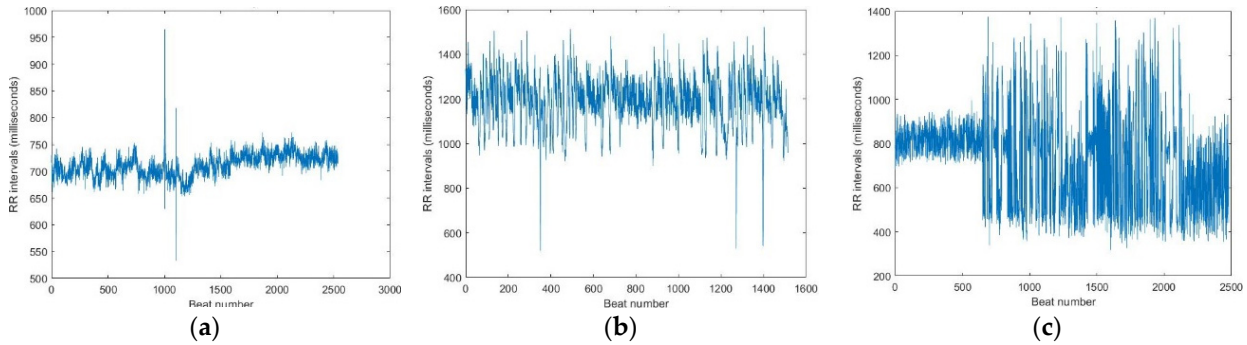

Figure 18. RR intervals vs. beat no. plots of recordings no. (**a**) 112, (**b**) 123, and (**c**) 222.

Figure 18 shows accurate RR interval plots, with higher variations in the RR intervals due to the recordings themselves, not missing R peaks. These variations lead to high-magnitude events in the LF and HF regions, as seen in the spectrograms in Figure 19, suggesting an unexpected LF/HF ratio. At the power estimation stage (Table 4), the LF/HF ratio for these recordings was higher than one, deviating from other arrhythmia recordings.

Recording no. 16,539, shown in Figure 20a, exhibited bright LF and VLF ranges typical of normal sinus rhythm, along with bright spots in the HF range after 35 min. The RR interval plot (Figure 20b) shows that the variations are due to the recording, not missing R peaks. However, the power estimation (Table 5) indicated a lower LF/HF ratio than

one, deviating from other normal sinus recordings due to the higher magnitudes in the HF band.

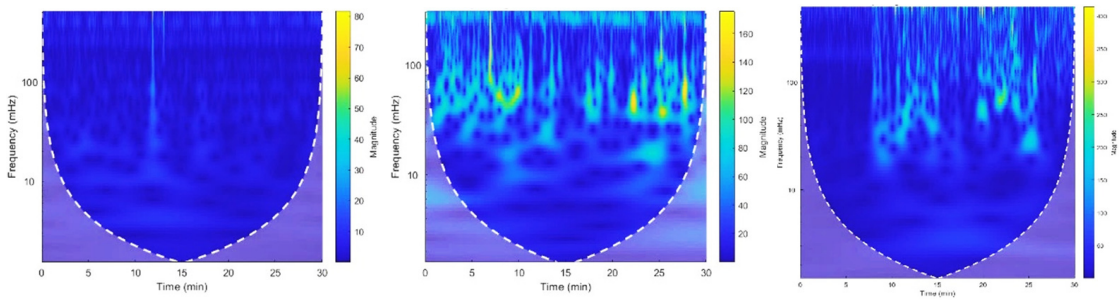

(**a**) (**b**) (**c**)

Figure 19. CWT spectrograms of recordings no. (**a**) 112, (**b**) 123, and (**c**) 222.

Table 4. Estimated power values for MIT-BIH Normal Sinus Rhythm dataset.

Record No.	Power (ms^2)			Total Power	Normalized Power (n.u)			LF/HF Ratio
	VLF	LF	HF		VLF	LF	HF	
16,265	982.206	797.42	251.961	2031.588	0.483	0.392	0.124	3.164
16,272	3695.852	871.607	334.761	4902.22	0.753	0.177	0.068	2.603
16,273	1923.648	613.323	213.616	2750.588	0.699	0.222	0.077	2.871
16,420	497.22	634.57	56.026	1187.818	0.418	0.534	0.047	11.326
16,483	505.501	648.268	81.5	1235.27	0.409	0.524	0.065	7.954
16,539	2869.741	1244.762	2916.094	7010.597	0.409	0.174	0.415	0.42
16,773	3323.282	2259.39	775.58	6358.26	0.522	0.355	0.121	2.913
16,786	1284.794	1068.521	569.724	2923.039	0.439	0.365	0.194	1.875
16,795	4178.642	1943.284	1074.122	7196.048	0.58	0.27	0.149	1.809
17,052	3553.84	1132.412	6411.643	5327.416	0.667	0.212	0.12	1.766
17,453	1568.02	1000.653	3384.886	2907.171	0.539	0.344	0.116	2.956
18,177	1150.257	749.455	441.022	2340.735	0.491	0.320	0.188	1.699
18,184	2325.916	1015.988	2211.593	3563.063	0.652	0.285	0.062	4.593
19,088	727.481	366.368	231.762	1325.611	0.548	0.276	0.174	1.58
19,090	1194.602	617.317	144.911	1956.831	0.61	0.315	0.074	4.259
19,093	3770.705	1456.669	325.436	5552.81	0.679	0.262	0.058	4.476
19,140	806.541	479.895	280.741	1567.178	0.514	0.306	0.179	1.709
19,830	247.947	85.615	22.06	365.63	0.678	0.261	0.06	4.332

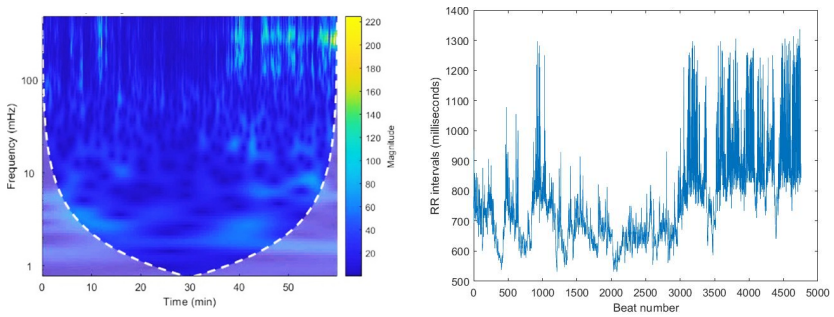

(**a**) (**b**)

Figure 20. (**a**) CWT spectrograms and (**b**) RR intervals vs. beat no. plots of recording no. 16,539.

Table 5. Estimated power values for MIT-BIH Arrhythmia dataset.

Index	Power (ms^2)			Total Power	Normalized Power (n.u)			LF/HF Ratio
	VLF	LF	HF		VLF	LF	HF	
100	295.895	136.511	863.592	1295.999	0.228	0.105	0.666	0.158
101	740.593	508.507	967.957	2217.058	0.334	0.229	0.436	0.525
103	874.086	283.325	619.681	1777.093	0.491	0.159	0.348	0.457
105	278.359	291.088	1080.02	1649.463	0.168	0.176	0.654	0.269
106	4155.21	1863.38	18,948.4	24,967	0.166	0.074	0.758	0.098
107	83.027	275.126	904.511	1262.666	0.065	0.217	0.716	0.304
108	2258	3386	7143	12,788	0.176	0.264	0.558	0.474
109	225.357	55.861	506.856	788.076	0.285	0.07	0.643	0.11
111	248.827	179.993	728.289	1157.111	0.215	0.155	0.629	0.247
112	108.338	37.878	36.819	183.036	0.591	0.206	0.201	1.02
113	2017.82	2532.15	4264.53	8814.49	0.228	0.287	0.483	0.593
114	836.476	788.307	5093.99	6718.77	0.125	0.117	0.758	0.154
115	3063.9	1841.02	1896.19	6801.099	0.45	0.27	0.278	0.97
116	267.311	574.905	1630.48	2472.701	0.108	0.232	0.659	0.352
117	1026.8	222.463	261.004	1510.326	0.679	0.147	0.172	0.852
118	898.244	699.618	1809.2	3407.059	0.263	0.205	0.531	0.386
119	966.203	1168.92	21,469.9	23,605	0.04	0.049	0.909	0.054
121	847.944	171.545	205.958	1225.449	0.691	0.139	0.168	0.832
122	928.243	128.752	71.893	1128.889	0.822	0.114	0.063	1.79
123	4304.29	6332.78	2945.29	13,582.36	0.316	0.466	0.216	2.15
124	1353.45	435.352	1467.37	3256.174	0.415	0.133	0.45	0.296
200	691.461	881.709	3113.06	4686.227	0.147	0.188	0.664	0.283
201	22,255	13,128.3	31,395.5	66,778.85	0.333	0.196	0.47	0.418
202	4171.18	3406.07	8072.44	15,649.7	0.266	0.217	0.515	0.421
205	128.279	81.507	378.745	588.532	0.217	0.138	0.643	0.215
209	2886.21	580.797	769.583	4236.593	0.681	0.137	0.181	0.754
210	1139.49	2012.61	4775.11	7927.211	0.143	0.253	0.602	0.421
212	345.922	380.276	539.868	1266.067	0.273	0.3	0.426	0.704
213	15.81	53.506	173.516	243.834	0.068	0.219	0.711	0.308
214	2396.8	3278.84	9936.07	15,611.7	0.153	0.21	0.636	0.329
215	80.294	229.978	924.845	1235.119	0.065	0.186	0.748	0.248
217	661.746	749.83	2301.01	3712.586	0.178	0.201	0.619	0.325
220	1865.91	1179.83	3409.84	6455.575	0.289	0.182	0.528	0.346
221	1636.79	4791.15	15,135.5	21,563.49	0.075	0.222	0.701	0.316
222	6280.23	12,581.8	8126.31	26,988.38	0.232	0.466	0.301	1.54
223	649.899	333.746	971.99	1955.637	0.332	0.17	0.497	0.343
228	1758.14	2596.81	8272.69	12,627.64	0.139	0.205	0.655	0.313
230	1894.66	991.77	308.061	3194.425	0.593	0.31	0.096	3.21
231	33,216.2	4396.81	3197.72	40,810.67	0.813	0.107	0.078	1.38
232	14,254.9	111,483	221,810	347,547.8	0.041	0.32	0.638	0.502

Table 5. *Cont.*

Index	Power (ms^2)			Total Power	Normalized Power (n.u)			LF/HF Ratio
	VLF	LF	HF		VLF	LF	HF	
233	122.723	1905.31	1998.67	23,119.26	0.053	0.082	0.864	0.095
234	393.933	113.916	167.856	675.706	0.582	0.168	0.248	0.678

Missing R peaks, leading to incorrect higher RR intervals, can also be seen as high-magnitude events in spectrograms. For example, Figure 21 shows a high magnitude between 15 and 20 min in the HF range due to a missing R peak, causing the overall spectrogram to appear dimmer. This condition is observed in all six recordings with missing R peaks.

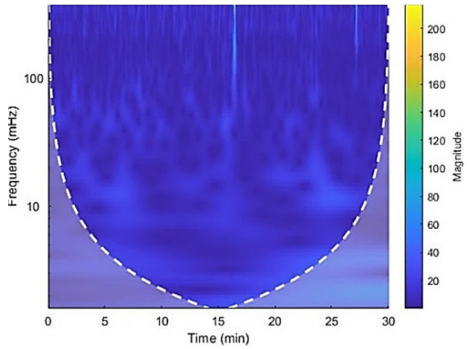

Figure 21. CWT spectrograms of recording no. 121.

The CWT spectrograms of some recordings, such as Figure 22a, show high magnitudes throughout, while others, like Figure 22b, display reduced brightness. This variation is due to each person having a unique ECG pattern, influenced by the structure of their heart, causing differences in signal magnitude and intensity [37].

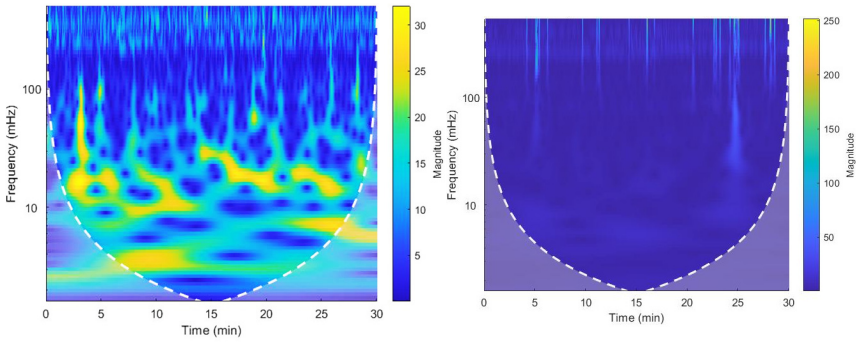

(**a**) (**b**)

Figure 22. CWT spectrograms of recordings no. (**a**) 122 and (**b**) 205.

The next step involved extracting frequency bands (VLF, LF, and HF) using inverse CWT, with frequency ranges set as VLF (0.003–0.04 Hz), LF (0.04–0.15 Hz), and HF (0.15–0.4 Hz) for long-term ECG recordings [36]. The power of these bands was calculated by taking the square of the RMS values of the reconstructed signals, and power values were normalized to compare their contribution to total power. The LF/HF ratio was computed to assess the sympatho-vagal balance of the ANS. The power estimates are summarized in Tables 4 and 5.

While the LF and HF bands are the main focus for the LF/HF ratio, the VLF band also contributes significantly to total power. The LF band is believed to reflect both sympathetic

and parasympathetic activity, while the HF band reflects parasympathetic activity [38–40], though some studies suggest the LF band represents sympathetic activity [41,42]. However, the LF/HF ratio is considered an indicator of the sympatho-vagal balance of ANS activity [43–45].

The power estimates for the Normal Sinus Rhythm dataset in Table 4 show that normalized HF power is lower than LF power in most recordings, suggesting better activity in the LF range, potentially leading to an LF/HF ratio greater than one.

Recording no. 16,539 shows an LF/HF ratio of 0.42, the lowest observed in Table 4. Unlike the other recordings, this one has a higher normalized power for the HF band than the LF band, resulting in a lower LF/HF ratio. The RR interval plot of this recording exhibited significant variation in the RR intervals, likely due to the variations in the ECG recording itself. This suggests that high HRV could lead to a lower LF/HF ratio, and the subject might have an undiagnosed heart condition or arrhythmia, though no conclusion can be made.

For recordings no. 16,420 and 16,483, the LF/HF ratio was much higher than in the other recordings due to missing R peaks, which caused incorrect higher RR intervals. The estimated normalized HF power was very low, while the LF power was higher. The spectrograms showed high-magnitude events in the HF region that spread into the LF range, leading to a higher LF/HF ratio [46,47].

The estimated power values for the Arrhythmia dataset are shown in Table 5. In most cases, the normalized LF power is lower than the normalized HF power, indicating better activity in the HF range compared to LF. Except for six recordings, most LF/HF ratios were lower than one, and the ratios in the Arrhythmia dataset were generally lower than those in the normal sinus dataset.

Recordings no. 106, 119, and 233 have very low LF/HF ratios, with abnormally low LF power compared to HF power. In the RR interval calculation step, large variations were observed in these recordings, which also appear as high-magnitude events in the HF range in the spectrograms (Figures 23 and 24). These variations suggest that high HRV could lead to a lower LF/HF ratio.

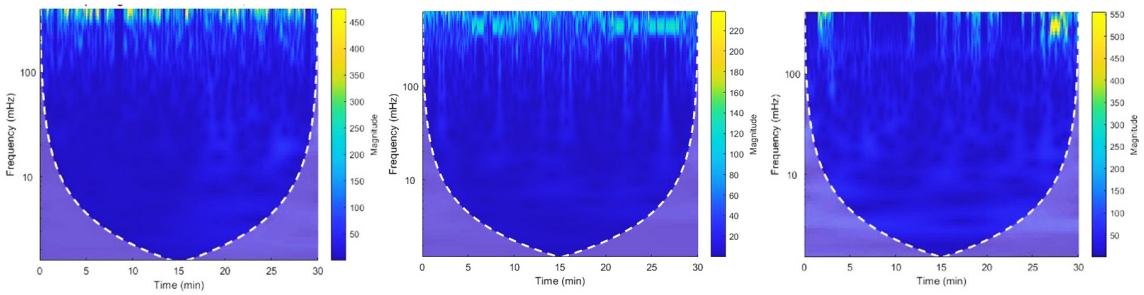

Figure 23. CWT spectrograms of recordings no. (**a**) 106, (**b**) 119, and (**c**) 233.

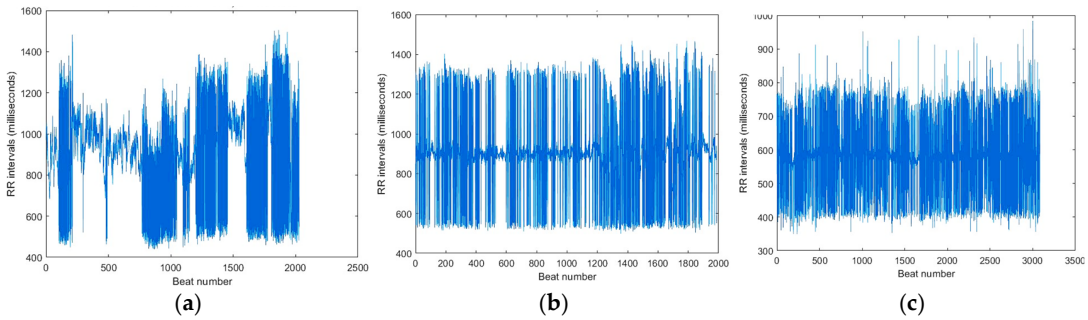

Figure 24. RR intervals vs. beat number plots of recordings no. (**a**) 106, (**b**) 119, and (**c**) 233.

For recordings no. 112, 122, 123, 222, 230, and 231, the LF/HF ratio was higher than one, as seen in the spectrograms (Figure 19). These recordings showed high-magnitude events in both the LF and HF ranges, with the LF events being brighter than HF. These variations were reflected in the RR interval plots and confirmed during power estimation, where the LF/HF ratio was higher than one, deviating from the other recordings.

To compare the LF/HF ratios between the Normal Sinus Rhythm and Arrhythmia datasets, scatter plots were created (Figure 25), illustrating the LF/HF ratios of both groups.

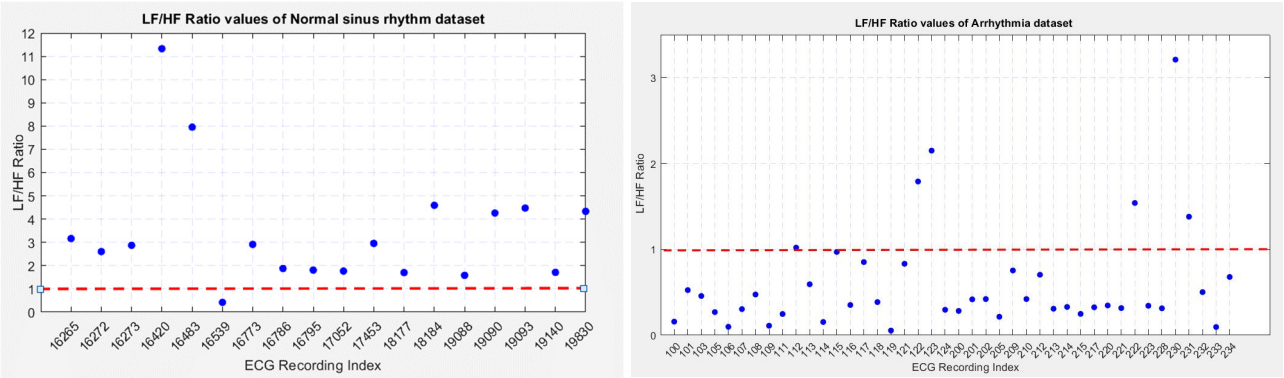

(**a**) (**b**)

Figure 25. Scatter plot of LF/HF values of (**a**) Normal Sinus Rhythm dataset and (**b**) Arrhythmia dataset.

Figure 25a shows the distribution of the LF/HF ratios for the normal sinus rhythm recordings, where most ratios are above one, except for recording no. 16,539, which deviated due to variations in the RR intervals. Recordings no. 16,420 and 16,483 showed higher ratios due to missing R peaks, causing incorrect high variations.

Figure 25b displays the LF/HF ratios for the arrhythmia recordings, with most ratios below one, except for six recordings. Recordings no. 112 and 115 had a ratio close to one, indicating balanced parasympathetic and sympathetic nervous system activity.

Anomalous recordings in both datasets were due to high variations in the RR intervals. In the Normal Sinus Rhythm dataset, recording no. 16,539 showed a low LF/HF ratio, while in the arrhythmia recordings, the high LF range power contributed to a higher LF/HF ratio. The comparison between both datasets shows that arrhythmia subjects are more likely to have a lower LF/HF ratio, indicating a dominance of the parasympathetic nervous system (PNS), while normal sinus rhythm subjects show a higher ratio, indicating sympathetic nervous system (SNS) dominance.

As a future work wavelet transform could be used in the HRV analysis of patients suffering from different kinds of diseases and it could also be used to study the effect of gender and age on HRV.

4. Conclusions

Heart rate variability (HRV) reflects cardiac activity and overall autonomic nervous system health. Proper HRV analysis aids in identifying diseases and managing heart conditions. Using ECG signals from the PhysioNet database, the HRV analysis employed the continuous wavelet transform (CWT) and discrete wavelet transform (DWT) methods.

R peaks localization was performed using DWT methods: MODWPT and MODWT. MODWPT outperformed MODWT due to superior signal decomposition but was not continued due to computational limitations. Seven out of 60 recordings had missing R peaks due to data loss during initial localization.

CWT was applied to RR interval signals to generate spectrograms, revealing patterns related to heart conditions In these spectrograms high magnitude events were spotted. In some spectrograms, the power of the HF range was dominant, this was commonly observed in the arrhythmia ECG recordings. In some other spectrograms, the power of the LF range was dominant, this was commonly observed in the normal sinus rhythm ECG recordings. The CWT spectrogram of some recordings exhibited high magnitudes all over the spectrogram, while some other recordings displayed a reduction in brightness throughout the spectrogram. The reason is that every person has a unique pattern in ECG due to the different structures of their hearts and therefore, the ECG signal can vary in magnitude, having low or high intensities depending on the person.

Frequency band extraction using ICWT reconstructed HF, LF, and VLF bands (0.003–0.5 Hz). Power estimation, calculated as the square of the RMS values of reconstructed signals, indicated significant differences in LF/HF ratios between the Normal Sinus Rhythm and Arrhythmia datasets. Normal sinus rhythm often showed abnormally low LF/HF ratios due to dominant HF power, while the Arrhythmia dataset exhibited abnormally high LF/HF ratios due to dominant LF power.

The scatter plot analysis confirmed lower LF/HF ratios in the Arrhythmia dataset, indicating parasympathetic dominance, whereas the Normal Sinus Rhythm dataset showed sympathetic dominance. This highlights the use of wavelet-based HRV analysis for distinguishing autonomic regulation patterns in cardiac health and disease.

As a future direction, taking a more statistical approach together with MODWPT-based HRV analysis will provide a more quantitative and reliable interpretation of HRV with deeper insight into the autonomic nervous system. Also, DWT feature extraction could improve with machine learning to enhance the interpretation of CWT spectrograms in HRV analysis.

Author Contributions: Writing—original draft, A.M.N.; Writing—review & editing, C.H.M.; Supervision, N.G.S.S.G.; Funding acquisition, T.N. All authors have read and agreed to the published version of the manuscript.

Funding: This research received no external funding.

Institutional Review Board Statement: Not applicable.

Informed Consent Statement: Not applicable.

Data Availability Statement: The original contributions presented in the study are included in the article, further inquiries can be directed to the corresponding author.

Conflicts of Interest: The authors declare no conflict of interest.

References

1. Berntson, G.G.; Bigger, J.T.; Eckberg, D.L.; Grossman, P.; Kaufmann, P.G.; Malik, M.; Nagaraja, H.N.; Porges, S.W.; Saul, J.P.; Stone, P.H.; et al. Heart rate variability: Origins, methods, and interpretive caveats. *Psychophysiology* **1997**, *34*, 623–648. [CrossRef] [PubMed]
2. Kim, H.-G.; Cheon, E.-J.; Bai, D.-S.; Lee, Y.H.; Koo, B.-H. Stress and heart rate variability: A meta-analysis and review of the literature. *Psychiatry Investig.* **2008**, *15*, 235–245. [CrossRef] [PubMed]
3. Hon, E. Electronic evaluations of the fetal heart rate patterns preceding fetal death: Further observations. *Am. J. Obstet. Gynecol.* **1965**, *87*, 814–826.
4. Kleiger, R.E.; Miller, J.P.; Bigger, J.T., Jr.; Moss, A.J. Decreased heart rate variability and its association with increased mortality after acute myocardial infarction. *Am. J. Cardiol.* **1987**, *59*, 256–262. [CrossRef]
5. Tsuji, H.; Venditti, F.J.; Manders, E.S.; Evans, J.C.; Larson, M.G.; Feldman, C.L.; Levy, D. Reduced heart rate variability and mortality risk in an elderly cohort. The Framingham Heart Study. *Circulation* **1994**, *90*, 878–883. [CrossRef] [PubMed]
6. Thayer, J.F.; Yamamoto, S.S.; Brosschot, J.F. The relationship of autonomic imbalance, heart rate variability and cardiovascular disease risk factors. *Int. J. Cardiol.* **2010**, *141*, 122–131. [CrossRef] [PubMed]

7. Carney, R.M.; Blumenthal, J.A.; Stein, P.K.; Watkins, L.; Catellier, D.; Berkman, L.F.; Czajkowski, S.M.; O'connor, C.; Stone, P.H.; Freedland, K.E. Depression, heart rate variability, and acute myocardial infarction. *Circulation* **2001**, *104*, 2024–2028. [CrossRef] [PubMed]
8. Gorman, J.M.; Sloan, R.P. Heart rate variability in depressive and anxiety disorders. *Am. Heart J.* **2000**, *140*, S77–S83. [CrossRef]
9. Chalmers, J.A.; Quintana, D.S.; Abbott, M.J.-A.; Kemp, A.H. Anxiety disorders are associated with reduced heart rate variability: A meta-analysis. *Front. Psychiatry* **2014**, *5*, 80. [CrossRef]
10. Abhishekh, H.A.; Nisarga, P.; Kisan, R.; Meghana, A.; Chandran, S.; Raju, T.; Sathyaprabha, T.N. Influence of age and gender on autonomic regulation of heart. *J. Clin. Monit. Comput.* **2013**, *27*, 259–264. [CrossRef]
11. Voss, A.; Schulz, S.; Schroeder, R.; Baumert, M.; Caminal, P. Methods derived from nonlinear dynamics for analysing heart rate variability. *Philos. Trans. R. Soc. A Math. Phys. Eng. Sci.* **2009**, *367*, 277–296. [CrossRef]
12. Agelink, M.W.; Malessa, R.; Baumann, B.; Majewski, T.; Akila, F.; Zeit, T.; Ziegler, D. Standardized tests of heart rate variability: Normal ranges obtained from 309 healthy humans, and effects of age, gender, and heart rate. *Clin. Auton. Res.* **2001**, *11*, 99–108. [CrossRef]
13. Umetani, K.; Singer, D.H.; McCraty, R.; Atkinson, M. Twenty-Four Hour Time Domain Heart Rate Variability and Heart Rate: Relations to Age and Gender Over Nine Decades. *J. Am. Coll. Cardiol.* **1998**, *31*, 593–601. [CrossRef]
14. Barantke, M.; Krauss, T.; Ortak, J.; Lieb, W.; Reppel, M.; Burgdorf, C.; Pramstaller, P.P.; Schunkert, H.; Bonnemeier, H. Effects of Gender and Aging on Differential Autonomic Responses to Orthostatic Maneuvers. *J. Cardiovasc. Electrophysiol.* **2008**, *19*, 1296–1303. [CrossRef] [PubMed]
15. Dinas, P.C.; Koutedakis, Y.; Flouris, A.D. Effects of active and passive tobacco cigarette smoking on heart rate variability. *Int. J. Cardiol.* **2013**, *163*, 109–115. [CrossRef]
16. Ralevski, E.; Petrakis, I.; Altemus, M. Heart rate variability in alcohol use: A review. *Pharmacol. Biochem. Behav.* **2019**, *176*, 83–92. [CrossRef]
17. Schnell, I.; Potchter, O.; Epstein, Y.; Yaakov, Y.; Hermesh, H.; Brenner, S.; Tirosh, E. The effects of exposure to environmental factors on Heart Rate Variability: An ecological perspective. *Environ. Pollut.* **2013**, *183*, 7–13. [CrossRef]
18. Elsenbruch, S.; Wang, Z.; Orr, W.C.; Chen, J.D.Z. Time-frequency analysis of heart rate variability using short-time Fourier analysis. *Physiol. Meas.* **2000**, *21*, 229–240. [CrossRef] [PubMed]
19. Acharya, U.R.; Joseph, K.P.; Kannathal, N.; Lim, C.M.; Suri, J.S. Heart rate variability: A review. *Med. Biol. Eng. Comput.* **2006**, *44*, 1031–1051. [CrossRef]
20. Boashash, B. *Time-Frequency Signal Analysis and Processing: A Comprehensive Reference*; Academic Press: Cambridge, MA, USA, 2015.
21. Daubechies, I. *Ten Lectures on Wavelets*; SIAM: Philadelphia, PA, USA, 1992.
22. Saxena, S.; Kumar, V.; Hamde, S. QRS detection using new wavelets. *J. Med. Eng. Technol.* **2002**, *26*, 7–15. [CrossRef]
23. Nouira, I.; Abdallah, A.B.; Kouaja, I.; Bedoui, M.H. Comparative study of QRS complex detection in ECG. *Int. J. Biomed. Biol. Eng.* **2012**, *6*, 593–597.
24. Nouira, I.; Abdallah, A.; Bedoui, M.H.; Dogui, M. A Robust R Peak Detection Algorithm Using Wavelet Transform for Heart Rate Variability Studies. *Int. J. Electr. Eng. Inform.* **2013**, *5*, 270–284. [CrossRef]
25. Li, C.; Zheng, C.; Tai, C. Detection of ECG characteristic points using wavelet transforms. *IEEE Trans. Biomed. Eng.* **1995**, *42*, 21–28. [CrossRef] [PubMed]
26. Zheng, H.; Wu, J. A Real-Time QRS Detector Based on Discrete Wavelet Transform and Cubic Spline Interpolation. *Telemed. e-Health* **2008**, *14*, 809–815. [CrossRef]
27. Mallat, S.G. A theory for multiresolution signal decomposition: The wavelet representation. *IEEE Trans. Pattern Anal. Mach. Intell.* **1989**, *11*, 674–693. [CrossRef]
28. Rioul, O. A discrete-time multiresolution theory. *IEEE Trans. Signal Process.* **1993**, *41*, 2591–2606. [CrossRef]
29. Pale, U.; Thürk, F.; Kaniusas, E. Heart rate variability analysis using different wavelet transformations. In Proceedings of the 2016 39th International Convention on Information and Communication Technology, Electronics and Microelectronics (MIPRO), Opatija, Croatia, 30 May–3 June 2016. [CrossRef]
30. Acharya, U.R.; Vidya, K.S.; Ghista, D.N.; Lim, W.J.E.; Molinari, F.; Sankaranarayanan, M. Computer-aided diagnosis of diabetic subjects by heart rate variability signals using discrete wavelet transform method. *Knowl.-Based Syst.* **2015**, *81*, 56–64. [CrossRef]
31. Ergen, B. Comparison of Wavelet Types and Thresholding Methods on Wavelet Based Denoising of Heart Sounds. *J. Signal Inf. Process.* **2013**, *4*, 164–167. [CrossRef]
32. Goldberger, A.L.; Amaral, L.A.N.; Glass, L.; Hausdorff, J.M.; Ivanov, P.C.; Mark, R.G.; Mietus, J.E.; Moody, G.B.; Peng, C.-K.; Stanley, H.E. PhysioBank, PhysioToolkit, and PhysioNet: Components of a New Research Resource for Complex Physiologic Signals. *Circulation* **2000**, *101*, E215–E220. [CrossRef] [PubMed]
33. Moody, G.B.; Mark, R.G. The impact of the MIT-BIH Arrhythmia Database. *IEEE Eng. Med. Biol. Mag.* **2001**, *20*, 45–50. [CrossRef] [PubMed]
34. Elgendi, M.; Jonkman, M.; De Boer, F. Frequency Bands Effects on QRS Detection. *Biosignals* **2010**, *2003*, 2002.

35. Cartas-Rosado, R.; Becerra-Luna, B.; Martínez-Memije, R.; Infante-Vázquez, Ó.; Lerma, C.; Pérez-Grovas, H.; Rodríguez-Chagolla, J.M. Continuous wavelet transform based processing for estimating the power spectrum content of heart rate variability during hemodiafiltration. *Biomed. Signal Process. Control* **2020**, *62*, 102031. [CrossRef]
36. Malik, M.; Bigger, J.T.; Camm, A.J.; Kleiger, R.E.; Malliani, A.; Moss, A.J.; Schwartz, P.J. Heart rate variability: Standards of measurement, physiological interpretation, and clinical use. *Eur. Heart J.* **1996**, *17*, 354–381. [CrossRef]
37. Dar, M.N.; Akram, M.U.; Usman, A.; Khan, S.A. ECG biometric identification for general population using multiresolution analysis of DWT based features. In Proceedings of the 2015 Second International Conference on Information Security and Cyber Forensics (InfoSec), Cape Town, South Africa, 15–17 November 2015. [CrossRef]
38. Hernando, A.; Posada-Quintero, H.; Peláez-Coca, M.D.; Gil, E.; Chon, K.H. Autonomic Nervous System characterization in hyperbaric environments considering respiratory component and non-linear analysis of Heart Rate Variability. *Comput. Methods Programs Biomed.* **2022**, *214*, 106527. [CrossRef]
39. Pomeranz, B.; Macaulay, R.J.; Caudill, M.A.; Kutz, I.; Adam, D.; Gordon, D.; Kilborn, K.M.; Barger, A.C.; Shannon, D.C.; Cohen, R.J.; et al. Assessment of autonomic function in humans by heart rate spectral analysis. *Am. J. Physiol. Circ. Physiol.* **1985**, *248*, H151–H153. [CrossRef] [PubMed]
40. Appel, M.L.; Berger, R.D.; Saul, J.; Smith, J.M.; Cohen, R.J. Beat to beat variability in cardiovascular variables: Noise or music? *J. Am. Coll. Cardiol.* **1989**, *14*, 1139–1148. [CrossRef] [PubMed]
41. Malliani, A.; Pagani, M.; Lombardi, F.; Cerutti, S. Cardiovascular neural regulation explored in the frequency domain. *Circulation* **1991**, *84*, 482–492. [CrossRef] [PubMed]
42. Montano, N.; Ruscone, T.G.; Porta, A.; Lombardi, F.; Pagani, M.; Malliani, A. Power spectrum analysis of heart rate variability to assess the changes in sympathovagal balance during graded orthostatic tilt. *Circulation* **1994**, *90*, 1826–1831. [CrossRef] [PubMed]
43. Houston, T.P.; Elster, A.B.; Davis, R.M.; Deitchman, S.D. The US Preventive Services Task Force Guide to Clinical Preventive Services, AMA Council on Scientific Affairs. *Am. J. Prev. Med.* **1998**, *14*, 374–376. [CrossRef]
44. Sztajzel, J. Heart rate variability: A noninvasive electrocardiographic method to measure the autonomic nervous system. *Swiss Med. Wkly.* **2004**, *134*, 514–522. [CrossRef]
45. Pagani, M.; Lombardi, F.; Guzzetti, S.; Rimoldi, O.; Furlan, R.; Pizzinelli, P.; Sandrone, G.; Malfatto, G.; Dell'Orto, S.; Piccaluga, E. Power spectral analysis of heart rate and arterial pressure variabilities as a marker of sympatho-vagal interaction in man and conscious dog. *Circ. Res.* **1986**, *59*, 178–193. [CrossRef] [PubMed]
46. German-Sallo, Z. Wavelet Transform based HRV Analysis. *Procedia Technol.* **2014**, *12*, 105–111. [CrossRef]
47. Shaffer, F.; Ginsberg, J.P. An Overview of Heart Rate Variability Metrics and Norms. *Front. Public Health* **2017**, *5*, 258. [CrossRef] [PubMed]